Lee and Lee *Int J Concr Struct Mater* (2025) 19:1
https://doi.org/10.1186/s40069-024-00748-y

International Journal of Concrete Structures and Materials

RESEARCH **Open Access**

Hysteresis Behavior of Reinforced Concrete Column Retrofitted and Repaired with Carbon Fiber Sheet

Moon-Sung Lee[1*] and Li-Hyung Lee[2]

Abstract

Structures experience damage and deterioration over their life cycle. The recent increase in interest in sustainable development of cities is re-evaluating the long-term use of structures. Therefore, researches on the retrofitting method for existing structures is receiving high attention again. However, there are very few cases where the direct comparison between the repair and retrofitting effects of structures has been experimentally verified. In this study, retrofitting methods and repair methods with carbon fiber sheets for reinforced concrete columns under shear failure were investigated. 10 reinforced concrete columns were tested under reversed cyclic loading. As a result of the experiment, it was found that, when reinforced with CFS strips, the increase in the width of the strip serves to enhance the strength and ductility of the reinforced member by providing confinement against shear cracks occurring in concrete. It was confirmed that as the number of overlaps of CFS increased, a greater strength-enhancing effect and ductility-enhancing effect appeared. However, the two-way reinforcement of CFS did not show a great effect in improving strength and ductility. As a result of evaluating the repair performance of damaged members using CFS, it was found that the strength and ductility of the repaired specimen exceeded the original strength and ductility of the base material as well as the strength and ductility of the reinforced specimen.

Keywords Carbon fiber sheet, Reinforced concrete column, Shear strengthening, Repairing

1 Introduction

Recently, as one of the methodologies for reducing the load of the construction industry on the environment, the demand for long-life buildings is increasing. Since buildings are subject to deterioration and damage during their life cycle, it is essential to find a suitable methodology for retrofitting structures in order to extend the life cycle of buildings. In particular, it is important to secure the ability of buildings to resist repeated natural disasters. This is because the secondary and tertiary earthquakes have a serious impact on the performance of structures, as already confirmed from the 1999 Kocaeli earthquake in Turkey and the 2010 and 2011 earthquakes in New Zealand. In particular, in the case of the New Zealand earthquake, after the first earthquake damaged the non-seismic detailed reinforced concrete structure, shear failure occurred in the columns of the lower part of the building due to the accumulated damage in the second earthquake [Sucuoglu, 2002; Uckan et al., 2002; Kam et al., 2011].

Non-seismic detailed reinforced concrete columns are particularly prone to shear failure as they have low shear strength. Methods that can be applied to increase the shear strength of non-seismic detailed reinforced concrete columns include section extension, steel plate

Journal information: ISSN 1976- 0485 / eISSN 2234-1315.

*Correspondence:
Moon-Sung Lee
moonlee@hanyang.ac.kr
[1] Division of Architecture and Architectural Engineering, Hanyang University, ERICA Campus, Ansan 15588, Korea
[2] Department of Architectural Engineering, Hanyang University, Seoul 04763, Korea

retrofitting, prestressing, and FRP jacketing. Among them, in the case of cross-section expansion or prestressing, there are restrictions on the use of indoor space after retrofitting, and in the case of steel plate reinforcement, problems with the integrity between the retrofitting materials and the original member and corrosion may occur. In addition, section expansion method and the steel plate retrofitting method entails an increase in weight.

FRP sheet has high strength-to-weight ratio and is stable against corrosion. In addition, the out-of-plane flexibility possessed by FRP sheet has the advantage of being applicable to various cross sections and providing convenience in construction. In addition, relatively fast construction speed can be an advantage in remodeling and repair projects.

Due to these advantages, the review of the structure of FRP has been steadily progressing from the end of the twentieth century to the present. Reinforcement using CFRP has the largest number of experimental histories among FRP reinforcement methods. As a result of previous studies [Ma et al., 2000; Ye et al., 2002], the reinforcement effect for non-seismic detail using CFRP was shown to be an improvement in both stiffness and ductility. In particular, there is also the study result of mechanically examining that CFRP sheet has a reinforcing effect on diagonal cracks [Ye et al., 2003]. Along with the study on the reinforcement of structural members using CFRP [Priestly & Seible, 1993; Saadatmanesh et al., 1997; Haroun et al., 2003; Khaloo, 2020], there are also research results on the repair using CFRP. A study on the repair of damage such as corrosion of rebar, cracking and spalling of yield concrete of reinforcing bar was conducted [Li & Sung, 2003; Guo et al., 2022; Yasir et al., 2022; Fakharifar et al., 2015; Yingwu et al., 2020; Fahmy et al., 2010]. In addition, recently, a study was conducted on the confinement effect of CFRP and the reinforcing effect caused by the embedding of reinforcing bars at the same time. [Hashemi et al., 2022]. As a result of the experiment, it was confirmed that an increase in strength and ductility can be expected at the same time when repaired with CFRP.

It was confirmed through past studies that the CFRP reinforcement effect is also related to the performance of the member to be reinforced. Therefore, in order to clearly evaluate the reinforcement effect, it is necessary to simultaneously review the CFRP reinforcement effect for undamaged members and the CFRP reinforcement effect for damaged members. However, it is difficult to find a case study that directly compares the reinforcement effect before and after damage.

Therefore, in this study, verification of the reinforcing effect of CFRP was first performed, and the degree of performance restoration of the damaged member was specified by checking the expression level of the reinforcing effect when damage occurred in the base material.

2 Design Equations for CFS Retrofitting

2.1 Shear Reinforcement Ratio

Kataoka et al. (1997) proposed a method of calculating the total reinforcement ratio by converting the amount of reinforcement to the amount of transverse reinforcement for a reinforced concrete column whose shear strength has been supplemented using CFRP. In this study, the following Eqs. (1) to (3) were used to define the amount of reinforcement:

$$\sum \rho_w(1) = {}_s\rho_w + {}_f\rho_w, \tag{1}$$

$$\Sigma\rho_w(2) = {}_s\rho_w + \frac{{}_fE}{{}_sE} \times {}_f\rho_w, \tag{2}$$

$$\Sigma\rho_w(1) = {}_s\rho_w + \frac{{}_f\sigma_w}{{}_s\sigma_w} \times {}_f\rho_w, \tag{3}$$

where $\Sigma\rho_w$ is total shear reinforcement ratio, ${}_s\rho_w$ is shear reinforcement ratio for rebar, ${}_f\rho_w$ is shear reinforcement ratio of CFS, ${}_fE$ is elastic modulus of CFS, ${}_sE$ is elastic modulus of rebar, ${}_f\sigma_w$ is tensile strength of cFS and ${}_s\sigma_w$ is yield strength of shear rebar.

2.2 Flexural Strength

For reinforced concrete columns with multiple layers of reinforcements, the Building Center of Japan (1997) and the Architectural Institute of Japan (1990) suggested the method calculating the ultimate flexural strength through the following equations:

when $N \leq 0.4bDf_{ck}$

$$M_u = 0.8a_{ts}\sigma_y D + 0.5ND\left(1 - \frac{N}{bDf_{ck}}\right), \tag{4}$$

when $N > 0.4bDf_{ck}$

$$M_u = \left(0.8a_{ts}\sigma_y D + 0.12D^2 f_{ck}\right)\left(\frac{N_{max} - N}{N_{max} - 0.4bDf_{ck}}\right), \tag{5}$$

where $N_{max} = bDf_{ck} + a_{gs}\sigma_y$, a_t is total area of longitudinal reinforcements(cm^2), D is total depth of column (cm), b is column width(cm), f_{ck} is compressive strength of concrete(kgf/cm^2), N is applied axial load(kgf), ${}_s\sigma_y$ is yield strength of steel rebar (kgf/cm^2) and a_g is total area of longitudinal reinforcement(cm^2).

2.3 Bond Strength

The Japanese Society of Architects also describes the evaluation of the bond behavior related strength of CFS retrofitted column [AIJ, 1998]:

$$Q_{sub} = \tau_{bu} \sum \psi j_t + \frac{tan\theta(1-\beta)bD\nu_c f_{ck}}{2} \leq bj_t \nu_c f_{ck}/2, \quad (6)$$

where $\tau_{bu} = \tau_{co} + \tau_{St}$, $\tau_{co} = \left[0.4\left\{(b - \Sigma d_b)/\Sigma d_b\right\} + 0.5\right]\sqrt{f_{ck}}$, when $N_t \leq 4$, $\tau_{st} = \left[\left\{\frac{(5N_t+10)}{N_t}\right\}\rho'_w b\sqrt{f_{ck}}\right]/d_b$, when $N_t > 4$, $\tau_{st} = 5\rho'_w b\sqrt{f_{ck}}/d_b$ N is number of longitudinal reinforcements on one layer, $tan\theta = \sqrt{(L/D)^2+1} - L/D$, $\beta = \left\{\tau_{bu}\sum\psi/(b\sin\phi\cos\phi)\right\}/(\nu_c f_{ck})$, $\rho'_w = {}_s\rho_w +_f \rho_w$ $\sum\psi$ is sum of circumferences of longitudinal reinforcement, j_t is spacing between rebar(cm), ν_c is effectiveness factor of compressive strength of concrete and it can be calculated by using $0.7 - f_{ck}/2000$, L is net height of the column (cm) Σd_b is summation of reinforcement diameter arranged with one layer.

2.4 Shear Strength

In calculating the shear strength of rectangular reinforced concrete columns reinforced with fiber sheets, the Japan Disaster Prevention Association uses the modified Hirosawa shear strength equation and revised the shear strength equation of the column suggested by AIJ to use the following two equations. Both equations are modified by converting the reinforcement amount of the fiber sheet into transverse reinforcement. In particular, Eq. (7) relates to a column on which a symmetrical moment acts when a horizontal load is applied:

$$Q_{su,1} = \left\{\frac{0.068\rho_t^{0.23}(180+f_{ck})}{M/Qd+0.12} + 2.7\sqrt{{}_sP_{ws}\sigma_w + \alpha_f P_{wf}\sigma_w} + 0.1\sigma_0\right\}.bj, \quad (7)$$

$$Q_{su,2} = bj_t\Sigma(P_w\sigma_w)cot\phi + tan\theta(1-\beta)\nu_c f_{ck}bD/2, \quad (8)$$

where $\Sigma(P_w\sigma_w) = {}_sP_{ws}\sigma_w + \alpha_f P_{wf}\sigma_w$, $\beta = \frac{\left\{(1+cot^2\phi)\Sigma(P_w\sigma_w)\right\}}{\nu_c f_{ck}}$, $cot\phi = \min\left\{2.0, \frac{j_t}{Dtan\theta}, \sqrt{\frac{\nu_c f_{ck}}{\Sigma(P_w\sigma_w)} - 1.0}\right\}$, $\frac{M}{Qd}$ is shear span-to-depth ratio, σ_0 is axial stress (kgf/cm^2), α is strength reduction factor, ρ_t is tensile reinforcement ratio (%), j length of moment arm, ϕ is angle of compressive strut of concrete.

3 Test Program

3.1 Variables and Specimen Detail

Experimental plan to examine the retrofitting effect of carbon fiber sheets on reinforced concrete columns with low level of shear strength when existing reinforced concrete structures do not meet the performance level required by the latest design standards or have experienced damage due to earthquakes, etc., was established. In this study, the occurrence and propagation of cracks, changes in load-bearing capacity, and safety were evaluated through the test for reinforced concrete columns under the lateral load. The specimens were largely divided into RC series, CF series, and RAD series. The RC-series specimens were constructed by adjusting the amount of shear reinforcement based on the shear-failure-type specimen and the flexural-failure-type specimen. For the CF-series specimens, the specimens were planned by adjusting the amount of reinforcement of the carbon fiber sheets in order to quantitatively evaluate the shear reinforcement effect on the shear fracture type RC columns. The RAD-series test specimens were to examine the repair effect of CFS on damaged reinforced concrete columns, and they were planned to have shear reinforcement that can experience the target displacement. The damage was determined based on the target displacement, and repair for the damage consisted of epoxy injection and CFS jacketing for cracks with a crack width of 0.2 mm or more. A total of 10 specimens were produced, with 3 RC-series specimens, 5 CF-series specimens, and 2 RAD-series specimens to check the reinforcing capacity of the carbon fiber sheet after damage.

Finally, each experimental group is classified according to the amount of shear reinforcement. For example, in the case of RC-015, 015 means that the shear reinforcement ratio is 0.15%. In the case of reinforcement with CFS, as can be seen in Table 1, it was calculated by adding the shear reinforcement amount of RC and the shear reinforcement amount of CFS.

All specimens were designed to have a square cross section of 300 × 300 mm and the height of all columns to be 900 mm. The main reinforcing bars of all specimens were arranged as 12-D13, and the amount of reinforcement of shear reinforcing bars and fibers was planned using the concept of shear reinforcing ratio. The specifications of each specimen are shown in Table 1, and the details of the specimen are shown in Fig. 1.

Table 1 Test specimens

Classification	Specimens ID	Shear reinforcement	CFRP layout			Shear reinforcement ratio (%)		
			Width [mm]	Number of layer	Direction	CFRP	Shear reinforcement	Total
RC	RC-015	ϕ6@130	–	–	–	–	0.151	0.151
	RC-059	*D*10@80	–	–	–	–	0.592	0.592
	RC-118	*D*10@40	–	–	–	–	1.183	1.183
CF	CF-026	ϕ6@130	40	1	HOR	0.0228	0.151	0.259
	CF-038	ϕ6@130	85	1	HOR	0.0484		0.381
	CF-050	ϕ6@130	900	1	HOR	0.0740		0.503
	CF-086	ϕ6@130	900	2	HOR	0.1480		0.856
	CF-VH	ϕ6@130	900	2	HOR + VER	0.0740		0.503
RAD	CF-RAD-200	ϕ6@130	900	1	HOR	0.0740		0.503
	CF-RAD-50	*D*10@80	900	1	HOR	0.0740	0.592	1.219

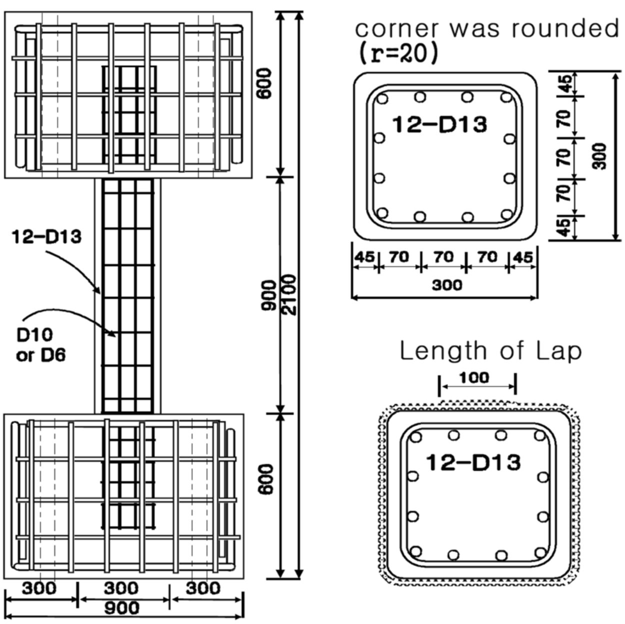

Fig. 1 Details of test specimens (unit: mm)

3.2 Materials

The compressive strength of the concrete used to manufacture the specimens was planned to be 27 MPa. The compressive load test of the concrete was performed according to KS F 2405 using a cylinder specimen with a diameter of 200 mm and a height of 100 mm [Korean Agency for Technology and Standards, 2006]. The 28-day compressive strength was 35.3 MPa and the elastic modulus was 24,231 MPa. At this time, the magnitude of the elastic modulus was determined by the slope determined by the stress at a strain of 50 μ and the stress at 1/3 stress of the maximum strength in the stress–strain curve. There were a total of three types of reinforcing bars used in the production of the specimens. The deformed reinforcing bar D13 was used as the longitudinal reinforcement, and the ϕ 6 round reinforcing bar and the D10 deformed reinforcing bar were used as the shear reinforcement. Each reinforcing bar was tested according to KS B 0802 [Korean Agency for Technology and Standards, 2007] and the test results are shown in Table 2.

The carbon fiber sheets used as the retrofitting material had an actual design thickness of 0.110 mm and a standard construction thickness of 0.45 mm. The tensile strength of the sheet was 3,482 MPa and the design modulus of elasticity was 230,535 MPa. The strain at fracture was found to be 1.5%.

3.3 Test Setup

The specimen was fastened to the reaction floor so that the base of the column could be completely fixed, and a guide frame and a ball jig were installed to prevent

Table 2 Mechanical properties of steel reinforcements

ID	Elastic modulus [*MPa*]	Yield strength [*MPa*]	Yield strain 10^{-6}	Tensile strength [*MPa*]	Elongation
ϕ6	195,219	721	3701	795	25.3
D10	178,547	412	2270	544	17.7
D13	167,751	455	2708	648	19.2

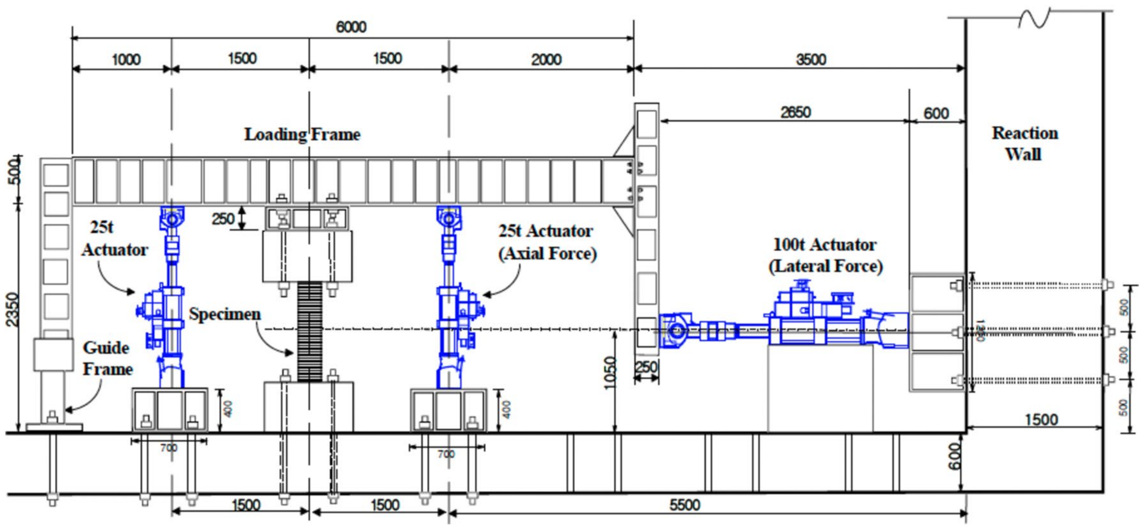

Fig. 2 Details of test set up (unit: mm)

out-of-plane deformation due to axial load while the lateral force was applied. As for the axial force, a load of $0.15f_{ck}A_g$ was applied in a load control method using actuators with a capacity of 250 kN installed on both sides of the specimen. The axial force allowed the same amount of load to be maintained during the experiment. Lateral load was applied at the midpoint of the column height so that a constant moment could act on the specimen using actuators with a capacity of 1000 kN.

The lateral force was applied through displacement control, and the lateral displacement of the specimen was controlled based on the member angle divided by the height of the loading point. It was gradually increased to the drift angles of 1/400, 1/200, 1/100, 1/67, 1/50, 1/33, 1/20, and 1/15 rad. Considering the amount of the longitudinal reinforcing bars of the specimens conducted in this study, 1/100 rad displacement angle at which yield is expected and 1/50 rad rotational angle at which the maximum load is expected were repeatedly applied twice.

The test setup plan and loading plan of the specimen are shown in Figs. 2 and 3, respectively.

4 Test Results and Analysis

4.1 Mode of Failure

The failure pattern of the test specimens were explained by dividing them based on the application of retrofitting method, the amount of reinforcement and repairing method. The RC-series specimens were reinforced only

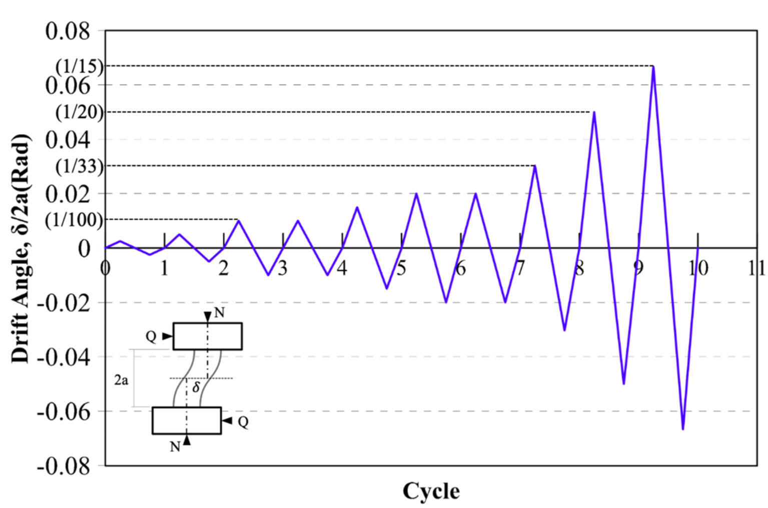

Fig. 3 Loading history

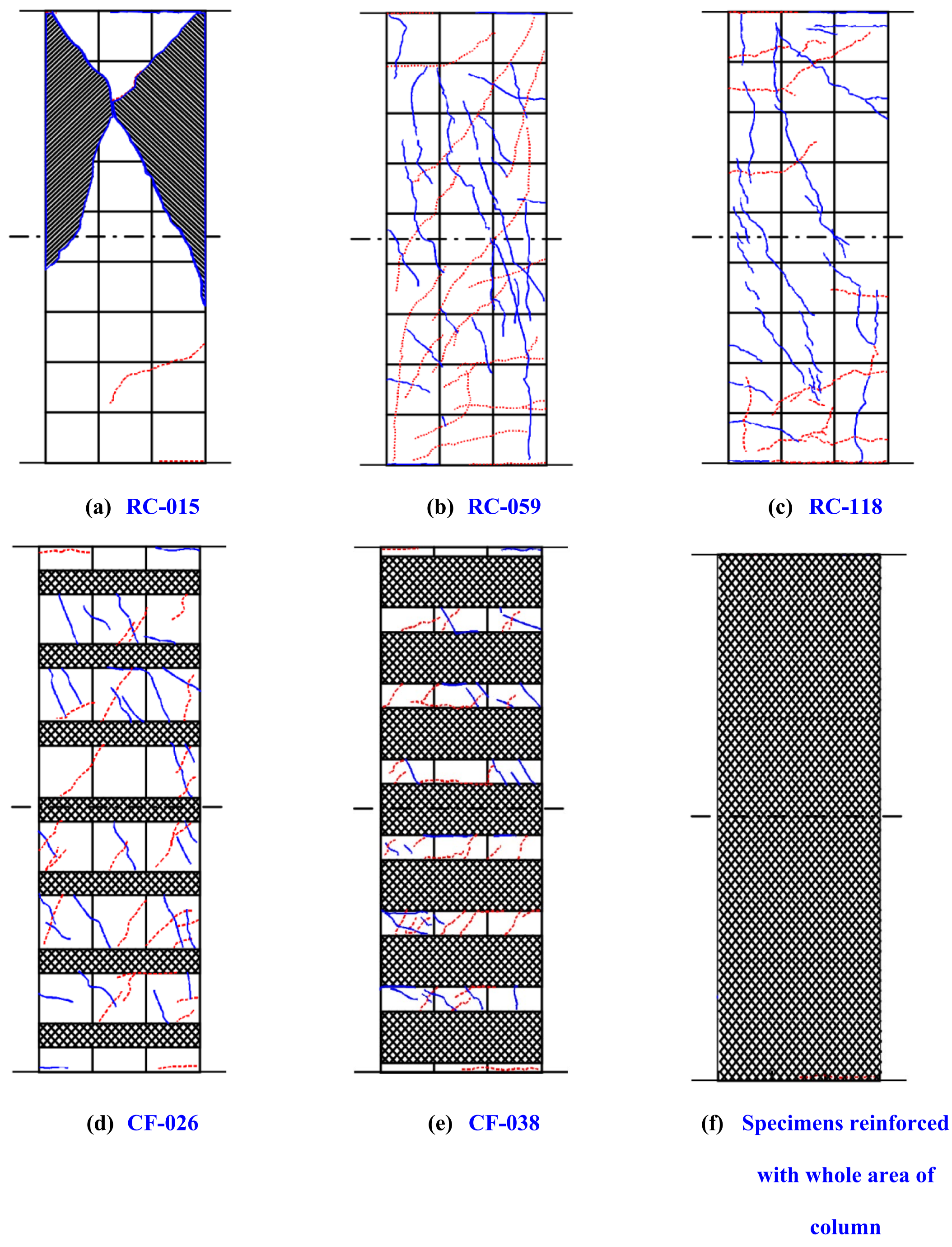

Fig. 4 Crack pattern of test specimens at the ultimate state

with shear rebars in the columns, and the failure pattern was changed according to the shear reinforcement ratio. The failure pattern of each specimen is shown in Fig. 4.

RC-015 was designed to be the lowest shear reinforcement ratio of 0.151%. A fine hair crack occurred at a displacement angle of 1/400 rad, and shear cracks occurred at the top of the column while experiencing a load of 189.3 kN at a displacement angle of 1/200 rad. After the shear crack in the opposite direction occurred at the pulling force of the corresponding displacement angle, it was finally failed with the sudden expansion of the shear crack width at 1/100 rad displacement angle.

RC-059 was reinforced with a shear reinforcement ratio of 0.592% with deformed reinforcing bars. It exhibited ductile behavior compared to RC-015. The initial flexural crack occurred at a rotational angle of 1/400 rad, and the flexural crack spread at a rotational angle of 1/200 rad. Shear cracks appeared while experiencing 1/100 rad rotational angle, and after damage was accumulated, cracks in the vertical direction were observed at the top end of the column along the direction of the longitudinal reinforcing bars at 1/67 rad rotational angle. As the negative force was experienced (pulling load), spalling of concrete spread and shear cracking progressed. At a rotational angle of 1/50 rad, the shear crack width was enlarged, and at a rotational angle of 1/20 rad, the shear crack width was rapidly enlarged and finally failed due to peeling off of concrete cover.

RC-118 has the largest shear reinforcement ratio in the RC series. Initial cracks occurred in the form of flexural cracks at a rotational angle of 1/200 rad. At 1/100 rad rotational angle, diagonal cracks occurred in the center of the column, but the development of flexural cracks was more pronounced. Afterwards, the propagation of flexural cracks were observed without the development of shear cracks until a rotational angle of 1/67 rad. At a rotational angle of 1/50 rad, the diagonal cracks began to spread, and crushing occurred at the end of the column. At 1/33 rad displacement angle, the crushing phenomenon accelerated, and at 1/20 rad rotational angle, the concrete collapsed at both ends of the upper column.

The CF-series specimens consist of specimens to investigate the retrofitting effect of the carbon fiber sheets. CFSs were attached on the column with same details of RC-015 specimen to confirm the effectiveness of retrofitting of CFS, where shear failure occurs predominantly. The width and thickness of CFS were changed to prepare various types of test specimens. Unlike the specimens with CFS strips, such as CF-026 and CF-038, cracks could not be observed for the specimens retrofitted through whole area of the columns. Therefore, there were no failure pattern observation results in Fig. 4 for specimens CF-050, CF-086, CF-VH, CF-RAD-200 and CF-RAD-50. The CFS strip was attached to the specimen so that the center line of the shear reinforcing bar and the center line of the strip coincide.

CF-026 was a specimen with 40-mm-wide sheets attached at 130-mm spacing, and shear cracks occurred at the top and bottom of the column at a rotational angle of 1/200 rad. At 1/100 rad rotational angle, flexural cracks occurred in the upper part, and cracks of about 60–70 mm occurred in the second upper sheet. Cracks with a length of 100 mm were also observed in the second lower sheet. Then, while experiencing the spread of shear cracks, concrete cover peeling cracks occurred at 1/67 rad rotational angle in the longitudinal rebar direction. After that, the accumulation of damage proceeded in the form of spread of shear cracks and peeling off of the concrete cover, and the sheet fractured at a rotational angle of 1/20 rad and finally failed.

CF-038 was a specimen with a sheet width of 85 mm. After initial flexural cracking at 1/200 rad rotational angle, shear cracking occurred at 1/100 rad rotational angle. As the hysteresis progressed, the shear crack spread and the length of the shear crack progressed at 1/67 rad rotational angle. At a rotational angle of 1/50 rad, a crack occurred in the sheet parallel to the sheet, and finally failed while experiencing fracture of the sheet at a rotational angle of 1/20 rad.

CF-050 was an entirely wrapped test specimen with CFS, and the sheet is made of one layer of CFS. Since the CFS covered the entire surface of the specimen, it was difficult to check the progress of the crack. However, it was confirmed that the upper and lower bending cracks occurred between the column and the loading beam at a rotational angle of 1/200 rad. At a rotational angle of 1/50 rad, the sheet peeling occurred at the top of the column, and at a rotational angle of 1/20 rad, the sheet peeling off at the upper part of the column occurred. In this case, delamination of the sheet progressed, leading to failure at 1/15 rad rotational angle.

CF-086 retrofitted with two layers of CFS. This specimen exhibited similar behavior to CF-050. The fracture was concentrated on the upper and lower parts of the column, discoloration occurred at 1/67 rad rotational angle, and the sheets at the upper and lower ends of the column fracture occurred at 1/20 rad and 1/15 rad rotational angles, resulting in final failure.

CF-VH was a specimen that was planned to examine the directional effect of the carbon fiber sheets. Flexural cracks first occurred at 1/100 rad rotational angle with the specimen retrofitted by one layer each in the horizontal and vertical directions. At 1/50 rad rotational angle, cracks occurred in the lower face of the column, and sheet fracture occurred at 1/33 rad of rotational angle. At a rotational angle of 1/15 rad, longitudinal cracking of the sheet in the vertical direction was confirmed, and the sheet was finally fractured as sheet peeling occurred one after another.

For RAD series specimens, the first and second loading stages were applied. During the first loading stage, damages at certain rotational angles were induced to the specimens. During the second loading stage, damaged test specimens were repaired with CFS wrapping and loaded again with the same loading history as shown in Fig. 3.

CF-RAD-200 is the same specimen as RC-015, and it was found to behave similarly to RC-015 up to a displacement angle of 1/200 rad. The main damage of RAD-200 was the initial flexural crack and the flexural shear crack that developed from this flexural crack. Among the cracks that occurred in the test specimen, cracks with a width of 0.2 mm or more were repaired with epoxy, and one-ply sheet wrapping was performed. The repaired specimen, CF-RAD-200, cracked first at the top and bottom of the column at 1/100 rad rotational angle. The sheet was damaged from a rotational angle of 1/67 rad, and some peeling off of the sheet occurred while experiencing a rotational angle of 1/33 rad and a rotational angle of 1/20 rad. At a rotational angle of 1/20 rad, the sheet peeled off, and test specimen was finally destroyed as it expanded to the top and bottom of the specimen at a rotational angle of 1/15 rad.

CF-RAD-50 is a specimen subjected to the force up to 1/50 rad rotational angle. The specimen experienced the propagation of flexure and flexural shear cracks occurring at rotational angles of 1/200 rad and 1/100 rad. At 1/50 rad rotational angle, shear cracks appeared in the center and the experiment was terminated. CF-RAD-50 retrofitted with CFS had cracks at the upper and lower ends of the column at a displacement angle of 1/200 rad, and then the damage to the carbon fiber sheet at the end was accumulated up to a rotational angle of 1/50 rad. After repeated loading for a rotational angle of 1/50 rad, crushing occurred at the bottom of the column, and the carbon fiber sheet was peeled off, and this phenomenon continued until the final fracture occurred.

P_{max}: maximum load applied to the specimen, P_y: yield load, $P_{y,r}$: load at the first yielding of flexural reinforcement, $\boldsymbol{\delta_{max}}$: displacement at maximum load,$\boldsymbol{\delta_y}$: displacement at yield load,$\boldsymbol{\delta_{y,r}}$: displacement at the first yielding of flexural reinforcement, δ_u: displacement at the load of $0.80P_{max}$

4.2 Load–Displacement Relation

Fig. 5 shows the load–displacement relationship of all specimens. Table 3 summarizes the yield strength and ultimate strength of each specimen and the corresponding displacement. At this time, the yield point of the member was determined through the method shown in Fig. 6.

The characteristics of each specimen are summarized as follows by dividing them into RC series, CF series, and RAD series as discussed about the failure mode. RC-015 is the specimen with the lowest shear reinforcement ratio, and after the member experienced yielding, it reached its maximum strength and experienced brittle shear failure that occurred at the same time. In the RC series, it was confirmed that the brittle behavior was alleviated as the shear reinforcement ratio increased. RC-059 showed a maximum load of 279.6 kN and experienced greater strength and greater displacement than RC-015. In relation to the failure mode, the failure occurred in a form induced from flexural failure to shear failure. RC-118 is a specimen in which shear failure is prevented by having a high shear reinforcement ratio. In the hysteresis curve, it was confirmed that large slip did not occur during unloading and loading. However, some problems occurred in the device for preventing out-of-plane displacement during the test of the specimen, resulting in a decrease in strength at 1/100 rad and 1/67 rad rotational angles. During the experiment, adjustments were made to the device, and it was confirmed that it showed a fracture form dominated by flexural failure.

CF series are test specimens to confirm the capability of CFS, and the effect of retrofitting was confirmed through retrofitting of RC-015, which showed brittle fracture. CF-026 is a member retrofitted by using a CFS with a width of 40 mm, and the CFS is attached in the form of a strip. The maximum load appeared at 1/100 rad rotational angle, and after experiencing the maximum load, it showed a large decrease in stiffness and strength. In addition, the pinching phenomenon occurred significantly in the hysteresis behavior. CF-038 was a test specimen with a strip width of 85 mm and exhibited the maximum bearing capacity at 1/100 rad rotational angle, and it was confirmed that the loss of load-bearing capacity occurred slower than CF-026.

Unlike CF-026 and CF-038, CF-050 was retrofitted by wrapping of CFS which is different from the general shear fracture type RC columns. The maximum load-bearing capacity was found to occur at 1/100 rad rotational angle, but it was confirmed that the degradation of the load-bearing capacity occurred gradually.

CF-086, to which the largest amount of reinforcement was applied, is a specimen in which two layers of carbon fiber sheets were wrapped in the horizontal direction. The test specimen's maximum load-bearing capacity reached its maximum at 1/100 rad rotational angle, but the load-bearing capacity was stably maintained up to 1/50 rad rotational angle, and as the pinching phenomenon was greatly improved, it did not experience a significant loss of load-bearing capacity up to 1/20 rad displacement angle. It was confirmed that the loss of load-bearing capacity was experienced less than 80% at 1/15 rad rotational angles. CF-VH was a specimen in which CFS were wrapped in two layers, but the CFS were arranged in an orthogonal direction. The maximum bearing strength of the specimen was found at 1/67 rad rotational angle, and the pinching phenomenon was improved compared to CF-050, but the maximum deformation capacity did not reach the deformation capacity of CF-050.

CF-RAD series were test specimens to verify the repair and retrofitting effects of CFS on damaged members. In

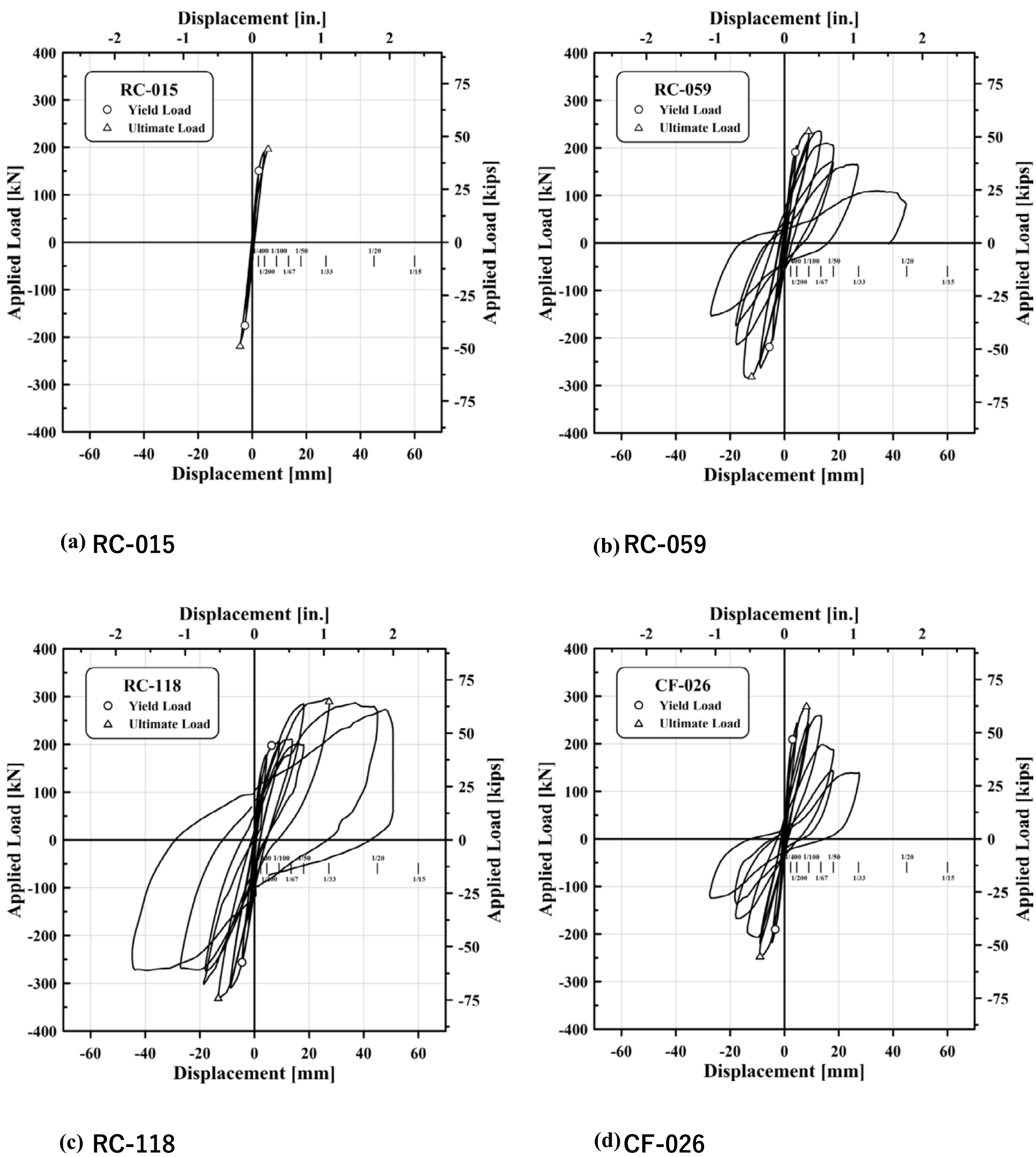

Fig. 5 Load–displacement relationship

the case of CF-RAD-200, it was confirmed that the effect on the damage of the member was a decrease in stiffness at the initial and maximum bearing capacity, and a stiff degradation of load-bearing capacity. In addition, it was confirmed that the pinching phenomenon was more pronounced than that of the CF-050. CF-RAD-50 has the same shear reinforcement details as RC-059 that had experienced rotational angles up to 1/50 rad. However, after the load-bearing capacity similar to the maximum bearing capacity appeared at 1/67 rad rotational angle, it experienced deformation up to 1/15 rad rotational angle without any decrease in the load-bearing capacity, and the hysteresis curve was changed from the shear fracture type to the flexural fracture type.

4.3 Ductility and Energy Dissipation

In order to compare and examine the ductility of each specimen, the ductility ratio was first defined. The ductility ratio was calculated based on the displacement at yield, the displacement at the maximum strength, and

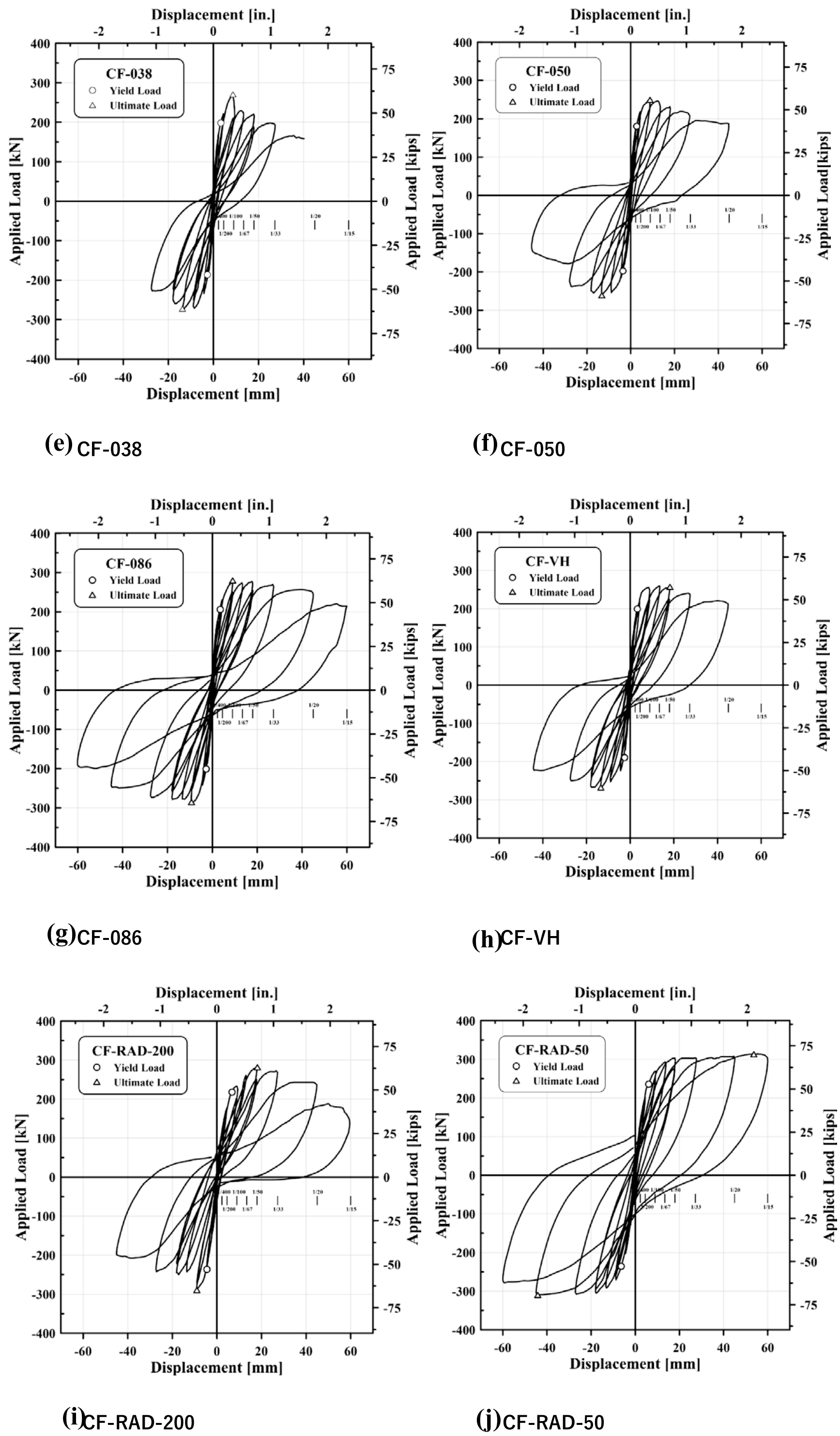

Fig. 5 continued

Table 3 Test results

ID		$P_{y,r}$ [kN]	$\delta_{y,r}$ [mm]	P_y [kN]	δ_y [mm]	P_{max} [kN]	δ_{max} [mm]	δ_u [mm]
RC-015	+	*	*	151.1	2.42	198.2	5.87	5.87
	−			−175.6	−2.67	−216.8	−4.47	−4.47
RC-059	+	225.6	6.815	191.3	3.95	236.4	8.90	18.19
	−			−218.8	−5.62	−279.6	−12.11	−15.01
RC-118	+	−309.0	−8.745	197.2	6.21	291.4	27.30	50.73
	−			−256	−4.57	−329.6	−13.32	−44.88
CF-026	+	279.6	8.115	209	3.00	279.6	8.12	13.53
	−			−190.3	−3.40	−245.3	−9.03	−13.51
CF-038	+	−266.8	−7.995	198.2	3.28	270.8	8.68	18.08
	−			−186.4	−2.69	−272.7	−13.75	−27.58
CF-050	+	−260.9	−13.200	180.5	2.75	249.2	8.80	27.02
	−			−197.2	−3.60	−260.9	−13.20	−27.78
CF-086	+	267.8	7.465	206	3.55	279.6	9.07	60.00
	−			−201.1	−2.78	−285.5	−9.32	−45.10
CF-VH	+	247.2	10.840	199.1	3.33	257.0	18.23	21.80
	−			−189.3	−2.53	−267.8	−13.40	−44.22
CF-RAD-200	+	218.8	11.505	217.8	6.76	281.5	18.12	45.00
	−			−236.4	−4.46	−289.4	−19.04	−27.28
CF-RAD-50	+	238.4	6.205	235.4	6.12	312.9	53.66	59.85
	−			−235.4	−6.37	−310.0	−44.17	−59.96

the displacement at the point where it decreased by 80% after the maximum strength as defined in Fig. 6 to summarize the experimental results. The displacement ductility ratio was calculated using Eq. (9).

$$\mu = \frac{\delta_{obj}}{\delta_y}, \tag{9}$$

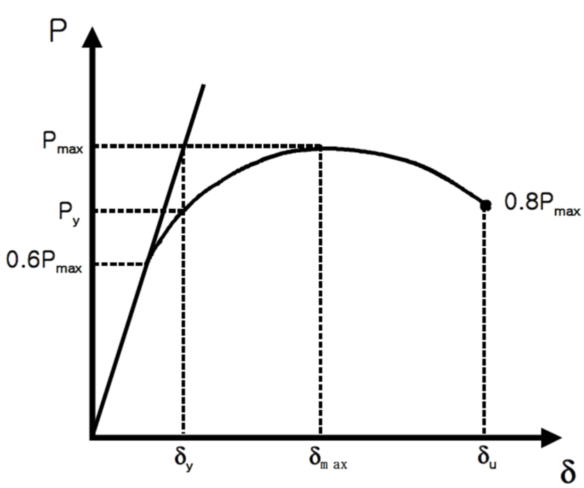

Fig. 6 Yielding of test specimens

where μ is displacement ductility ratio, δ_{obj} is objective displacement for calculating displacement ductility ratio and δ_y is displacement at yielding of test specimens.

Table 4 shows the displacement ductility ratios for both the positive and negative direction of loading because the displacement ductility ratios are different between the positive and negative forces. The displacement ductility ratio could be expressed in two ways: the ratio of the displacement during the experience of maximum strength to the yield displacement and the ratio of the ultimate displacement (displacement at 80% of the maximum load).

It can be confirmed that the change in the displacement ductility ratio of the RC-series specimens was directly affected by the amount of shear reinforcement, that is, the shear reinforcement ratio. The reason that the increase rate of the displacement ductility ratio for the ultimate state is higher than the increase rate of the displacement ductility ratio for the maximum strength is because the increase in the shear reinforcement ratio causes a change in the failure mode from shear failure to flexural failure. Therefore, in this section, the increase in the displacement ductility ratio with respect to ultimate strength is mainly considered.

Since all CF-series specimens were retrofitted specimens for specimens with the lowest displacement ductility among RC-series specimens, the ductility increase

Table 4 Displacement ductility factor

ID	μ_{peak}			μ_{ult}		
	Pos	Neg	Avg	Pos	Neg	Avg
RC-015	2.42	1.68	2.05	2.42	1.68	2.05
RC-059	2.25	2.16	2.205	4.60	2.67	3.635
RC-118	4.40	2.92	3.66	8.18	9.83	9.005
CF-026	2.71	2.65	2.68	4.51	3.97	4.24
CF-038	2.64	5.12	3.88	5.51	10.27	7.89
CF-050	3.21	3.67	3.44	9.84	7.73	8.785
CF-086	2.56	3.36	2.96	16.92	16.25	16.585
CF-VH	5.48	5.30	5.39	6.56	17.48	12.02
CF-RAD-200	2.68	2.03	2.355	6.65	6.12	6.385
CF-RAD-50	8.78	6.94	7.86	9.79	9.42	9.605

effect of carbon fiber sheets could be confirmed through CF-series specimens. As the displacement ductility ratio of the specimen increased in the order of CF-026 and CF-38, it was found that increasing the width of the strip plays an effective role in increasing the ductility ratio. When the test specimens were fully wrapped by CFS, the displacement ductility ratio of CF-050 wrapped with one layer increased to 428% compared to the behavior before retrofitting, and for CF-086, wrapped with two layers of CFS, it increased to 809%. In CF-VH, two layers of CFS were used, but the direction of the CFS was different. The increase in the displacement ductility ratio was 586% compared to the displacement ductility ratio of the base material. This is a smaller value than CF-086, which is reinforced with two layers in the same direction, which means that reinforcement in the same direction as the existing stirrup is more effective in enhancing ductility for the reinforcement of shear-failure-type members.

Looking at the specimens repaired by single layer wrapping of CFS, CF-RAD-200 increased by 311% compared to the displacement ductility ratio of the RC-015. Although this is a smaller value than the 428% increase in the displacement ductility ratio of the CF-026 which had no damage before loading, it was shown that a relatively large ductility can be secured even after repair and retrofitting. The displacement ductility ratio of CF-RAD-50 was 9.6, indicating that CF-RAD and CF-RAD-50 had a larger displacement ductility ratio to maximum strength.

The energy dissipation capacity is an important indicator that can be used to determine the deformability of the reinforced concrete members. The capability of the energy dissipation of the member that can be calculated by the area of the hysteresis curve when the cyclic loading experiment is performed is shown in Fig. 7. The retrofitting effect on the undamaged members is shown in Fig. 7a. It was confirmed that the early shear failure before reinforcement was greatly alleviated and high energy dissipation was maintained by retrofitting. As can be seen from 1/20 rad rotational angle at which the final fracture begins, the larger the strip width, the greater the energy dissipation, and it was confirmed that the largest energy dissipation amount could be secured for wrapping specimens. When double-layer wrapping was performed, it was confirmed that it has the ability to extend the deformation capacity. It caused the increase of energy dissipation capacity of the member.

The energy dissipation capacity of the repaired specimen was compared with that of the retrofitted specimen and shown in Fig. 7b. CF-RAD-200 was a specimen that had been repaired after damage applied to RC-015, and CF-RAD-50 was a specimen that had been repaired to a specimen with the same details as RC-059. It was confirmed that both specimens secured significantly improved energy dissipation capacity compared to the energy dissipation capacity of the specimen before failure. In particular, it was found that CF-RAD-50, which had been repaired for RC-059, can secure energy dissipation capability that surpasses the flexural behavior of the RC member. This is thought to be because CFS restrains the concrete from falling off. However, as the repaired specimen had damage, it was confirmed that the energy dissipation capacity was lower than that of the specimen to confirm the retrofitting ability before failure.

5 Retrofitting and Repairing Effect of CFS

5.1 Strain of Shear Reinforcements and CFS

To examine the shear strength increase effect of CFS, the strain of shear reinforcement and CFS are investigated as shown in Fig. 8. In Fig. 8a, the strain history of shear reinforcement and CFS at the upper position of the columns where shear cracks are concentrated was shown

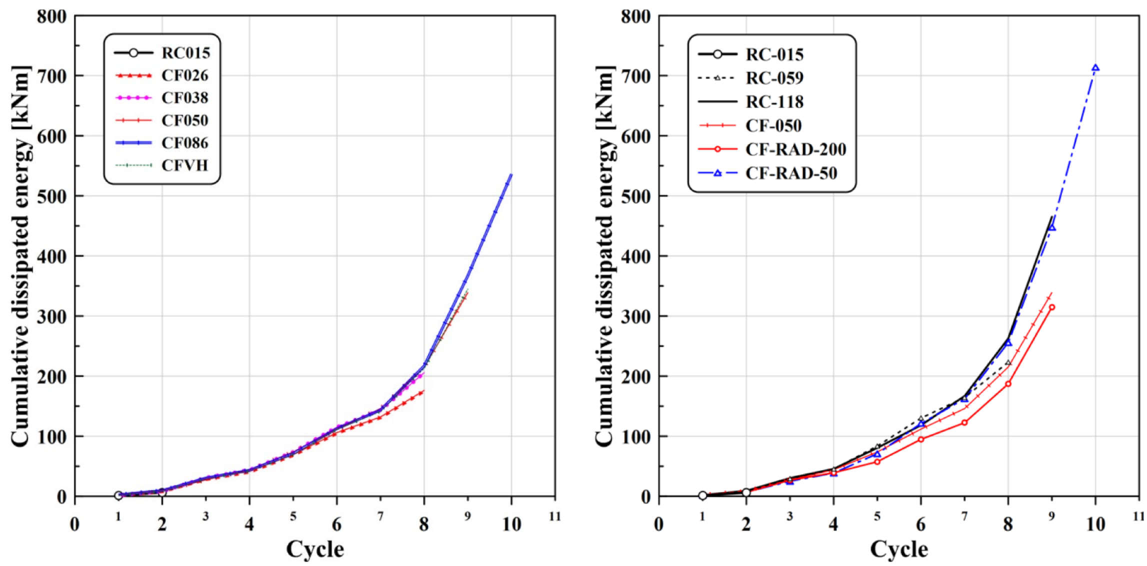

(a) Retrofitted specimens **(b) Repaired specimens**

Fig.7 Cumulative dissipated energy

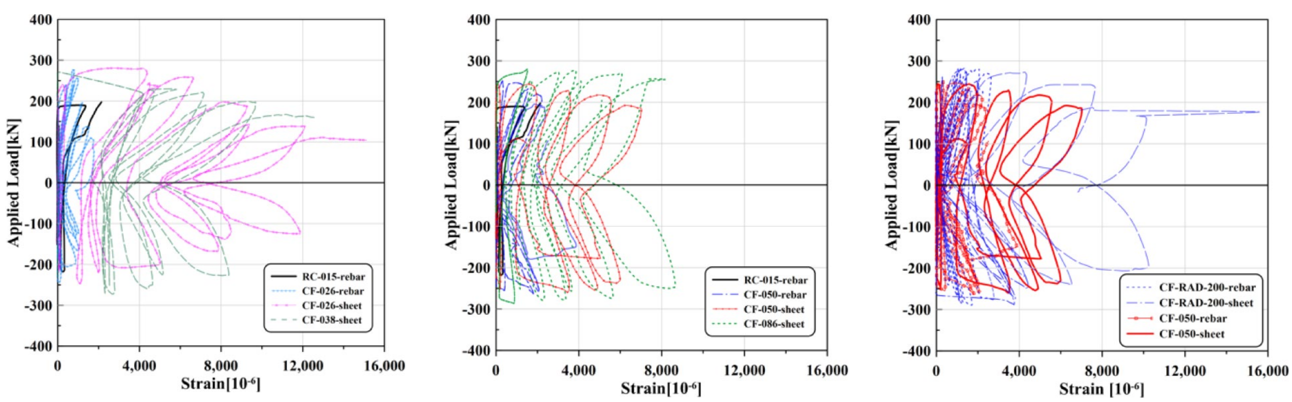

(a) Effect of width of CFS **(b)** Effect of CFS retrofitting method **(c)** Repairing effect of CFS

Fig. 8 Strain of CFS and shear reinforcements

in order to examine the retrofitting effect of the sheets. Among them, the wire strain gauge attached to shear rebars of CF-038 was dropped off prematurely during the test and thus could not be measured. In the case of RC-015, as can be seen from the failure mode and load–displacement curve, the shear reinforcements did not experience significant deformation due to shear failure. On the other hand, in the case of CF-026 reinforced with CFS of 40 mm width, the amount of deformation of the CFS increased, while the deformation of the reinforcing bars did not significantly increase and it was confirmed that the elastic state was maintained. This means that the main reinforcing mechanism of CFS directly prevents the crack width expansion. Fig. 8b shows the strain of the CFS sheets and reinforcing bars of the specimens. In the case of CF-086, the strain gauge attached to the

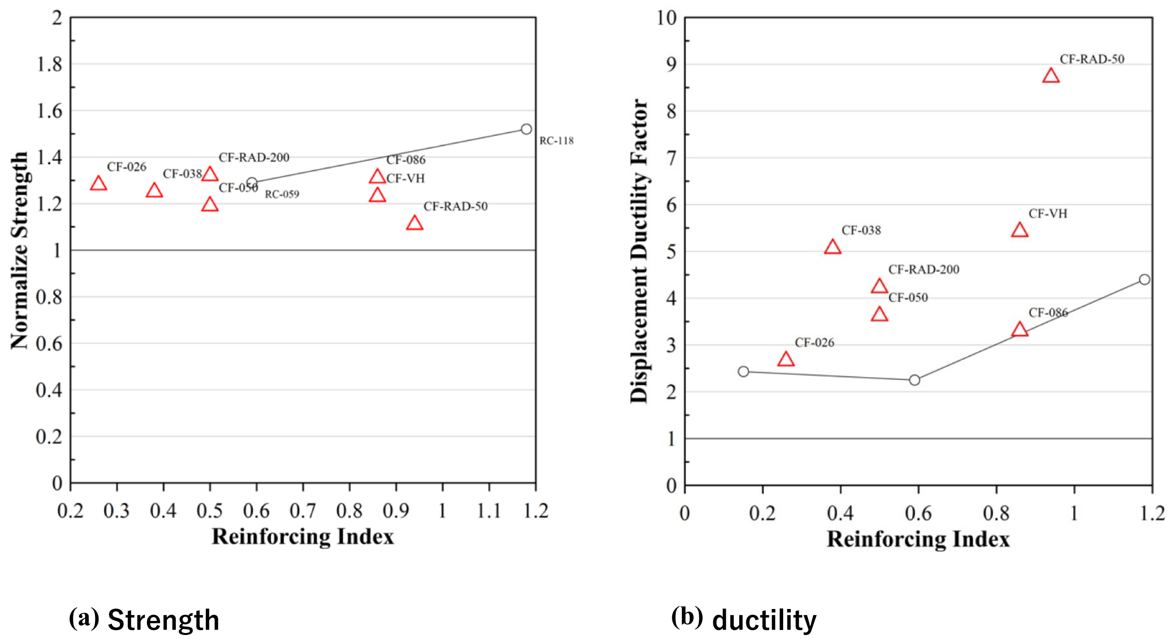

Fig. 9 Evaluation of strength and ductility of test specimens

reinforcing bars fell off. As shown in CF-026, the reason why the strain change of CFS was more prominent than that of reinforcing bars was considered to be because CFS was the element that firstly resists the expansion of crack width. It was confirmed that CFS experienced a large deformation even in CF-086, which had two layers of CFS.

To examine the repair effect of CFS in Fig. 8c, the shear reinforcement of CF-RAD-200 and the strain of CFS were compared with that of CF-050. In the case of CF-RAD-200, it was confirmed that the strain change of the shear reinforcement was related to the decrease in stiffness during the damage process by showing a larger strain at the initial stage of loading. Stiffness can be calculated by dividing the value of the maximum load for each cycle by the displacement under that load [Saadatmanesh et al., 1997]. However, it was confirmed that the behavior was similar to that of CF-RAD-200. The strain of CFS also showed a large strain at the beginning of loading, but it can be confirmed that the amount of strain of CFS after yielding of the member was smaller when repair is made. This is considered as a result of the increase in the internal rigidity of the member due to the epoxy injection.

5.2 Evaluation of Strength and Ductility

The change of strength and ductility according to the reinforcement ratio of the specimens are shown in Fig. 9a, b respectively. In order to understand the effect of reinforcement and repair according to the shear reinforcement ratio, the reinforcement ratio was calculated by using Eq. (3). The increase in strength of the repaired and retrofitted specimens compared to the RC-series specimens, which are the standard for retrofitting and repairing, was only up to 33%. On the other hand, it was confirmed that the deformation capacity was greatly improved in proportion to the amount of reinforcement. For CF-RAD-200, the maximum strength enhancement effect was confirmed, it was confirmed that the displacement ductility ratio for the extreme state increased by a maximum of 6.66 times. As can be seen from the comparison with RC-118, it is considered that the change in fracture mode is due to the fact that CFS played a role as a shear reinforcement until the development of flexural strength.

5.3 Evaluation of Existing Prediction Methods

In order to evaluate the prediction methods available for repair and retrofitted reinforced concrete columns using CFS, the predicted values calculated by Eqs. (4) to (8) and experimental results were compared. Table 5 summarizes the comparative results for each experimental result. Among them, the prediction result by Eq. (7) is shown with high accuracy. As a result of evaluation through the conversion equation of the strength reduction coefficient through Eq. (10), $\alpha = 1.0$ was suggested by using test results. However, Japan Disaster Prevention

Table 5 Prediction and evaluation of test specimens strength

ID	Q_{test} [kN]	$\alpha = 0.67$		$\alpha = 1.0$		Q_{su2} [kN]	$\frac{Q_{test}}{Q_{su2}}$	Q_{sub} [kN]	$\frac{Q_{test}}{Q_{sub}}$	Q_{bu} [kN]
		Q_{su1} [kN]	$\frac{Q_{test}}{Q_{su1}}$	Q_{su1} [kN]	$\frac{Q_{test}}{Q_{su1}}$					
RC-015	211.41	203.66	1.04	203.66	1.04	207.48	1.02	282.33	0.75	320
RC-059	258	259.18	1.00	259.18	1.00	295.28	0.87	324.71	0.79	
RC-118	310.49	305.58	1.02	305.58	1.02	418.49	0.74	381.51	0.81	
CF-026	262.42	216.02	1.21	221.31	1.19	235.73	1.11	284.49	0.92	
CF-038	271.74	227.59	1.19	237.11	1.15	267.42	1.02	287.04	0.95	
CF-050	272.23	246.53	1.10	261.93	1.04	329.71	0.83	291.85	0.93	
CF-086	255.06	237.7	1.07	250.45	1.02	299.11	0.85	289.49	0.88	
CF-VH	262.42	237.7	1.10	250.45	1.05	299.11	0.88	289.49	0.91	
CF-RAD-200	285.47	237.7	1.20	250.45	1.14	299.11	0.95	289.49	0.99	
CF-RAD-50	311.47	279.68	1.11	288.61	1.08	384.45	0.81	331.77	0.94	

Association suggested the value of 0.67 for α, two values were compared. Predicted value by using $\alpha = 1.0$ was more accurate than the value calculated by using $\alpha = 0.67$. However, relatively high accuracy also be secured by using $\alpha = 0.67$.

6 Conclusion

The conclusions obtained from the experiments conducted to evaluate the performance of the hysteresis characteristics and the maximum bearing capacity of the reinforced concrete columns shear-reinforced with carbon fiber sheets are as follows:

1) According to the test of this study, CFS retrofitting for reinforced concrete column can change the failure pattern of the reinforced concrete columns, especially from shear failure to flexural failure.
2) In the evaluation of the maximum shear strength of reinforced concrete columns retrofitted with CFS for the increasing shear strength of reinforced concrete columns, the strength reduction coefficient α for CFS was evaluated as 1.0 which was higher than the value 6.7 used in the shear strength formula of the Japan Disaster Prevention Association. This equation tends to underestimate the performance of reinforced concrete columns retrofitted by CFS.
3) It is thought that the shear retrofitting effect of CFS can be evaluated by using the method of reinforcing index suggested by AIJ.
4) It is judged that the minimum value obtained by comparing the shear strength equation, the bond strength equation, and the shear strength by flexural strength can evaluate the maximum shear strength of the columns well.
5) It was found that the stiffness and strength were not significantly affected by the increase or decrease in the amount of carbon fiber sheet reinforcement.
6) It was found that the energy dissipation capacity increased as the shear reinforcement ratio increased.
7) As the amount of reinforcement of CFS increased, the ductility ratio increased from 81 to 709% and the deformability from 162 to 920%, indicating that reinforcement of the carbon fiber sheet improved the ductility and deformability.

Acknowledgements

The research reported in this paper was supported by the advanced Structural RESearch Station (STRESS) of Korea Science and Engineering Foundation (KOSEF) at Hanyang University.

Author contributions

Moon Sung Lee: writing the manuscript, experimental works, data analysis, statistical analysis. Li Hyung Lee: writing the manuscript, data analysis, editing. All authors read and approved the final manuscript.

Funding

Advanced Structural RESearch Station (STRESS) of Korea Science and Engineering Foundation (KOSEF) at Hanyang University.

Availability of data and materials

Not applicable.

Declarations

Competing interests

Not applicable.

Received: 6 October 2022 Accepted: 1 February 2023
Published online: 01 February 2025

References

Architectural Institute of Japan. Design Guideline for Earthquake Resistant Reinforced Concrete Buildings Based on Ultimate Strength Concept, 1990

Architectural Institute of Japan Structural Committee. Application of Continuous Fiber Materials to Concrete Structures, Architectural Institute of Japan, 1998
Fahmy, M. F. M., Wu, Z., & Wu, G. (2010). Post-earthquake recoverability of existing RC bridge piers retrofitted with FRP composites. *Construction and Building Materials, 24*(6), 980–998.
Fakharifar, M., Chen, G., Sneed, L., & Dalvand, A. (2015). Seismic performance of post-mainshock FRP/steel repaired RC bridge columns subjected to aftershocks. *Composites Part B: Engineering, 72*, 183–198.
Guo, D., Gao, W.-Y., & Dai, J.-G. (2022). Effects of temperature variation on intermediate crack-induced debonding and stress intensity factor in FRP-retrofitted cracked steel beams: An analytical study. *Composite Structures, 279*, 114776.
Haroun, M. A., Mossalam, A. S., Feng, Q., & Elsanadedy, H. M. (2003). Experimental investigation of seismic repair and retrofit of bridge columns by composite jackets. *Journal of Reinforced Plastics and Composites., 22*(14), 1243–1268.
Hashemi, N., Hassanpour, S., & Vatani Oskoei, A. (2022). The effect of rebar embedment and CFRP confinement on the compressive strength of low-strength concrete. *International Journal of Concrete Structures and Materials, 16*, 17.
Kam, W. Y., Pampanin, S., & Elwood, K. (2011). Seismic performance of reinforced concrete buildings in the 22 February Christchurch (Lyttelton) earthquake. *Bulletin of the New Zealand Society for Earthquake Engineering., 44*(4), 239–278.
Khaloo, A., Tabatabaeian, M., & Khaloo, H. (2020). The axial and lateral behavior of low strength concrete confined by GFRP wraps: An experimental investigation. *Structures., 27*, 747–766.
Korean Agency for Technology and Standards. (2006). Method of test for splitting tensile strength of concrete. *KS F, 2423*, 1–12.
Korean Agency for Technology and Standards. (2007). Test pieces for tensile test for metallic materials. *KS B, 0801*, 1–18.
Li, Y. F., & Sung, Y. Y. (2003). Seismic repair and rehabilitation of a shear-failure damaged circular bridge column using carbon fiber reinforced plastic jacketing. *Canadian Journal of Civil Engineering., 30*(5), 819–829.
Ma, R., Xiao, Y., & Li, K. N. (2000). Full-scale testing of a parking structure column retrofitted with carbon fibre reinforced composites. *Construction and Building Materials, 14*, 63–71.
Priestly M. J. N, Seible F. Repair of shear column using fiberglass/epoxy jacket and epoxy injection. Report No. 93–04, Job No. 90–08, Seqad Consulting Engineers, Solana Beach, CA; c1993.
Saadatmanesh, H., Ehsani, M. R., & Jin, L. (1997). Repair of earthquake-damaged RC columns with FRP wraps. *ACI Structural Journal., 94*(2), 206–214.
Saeed, Y. M., Aules, W. A., & Rad, F. N. (2022). Post-strengthening rapid repair of damaged RC columns using CFRP sheets for confinement and NSM-CFRP ropes for flexural strengthening. *Structures, 43*, 1315–1333.
Sucuoglu, H. (2002). Engineering characteristics of the near-field strong motions from the 1999 Kocaeli and Duzce earthquake in Turkey. *Journal of Seismology., 6*(3), 347–355.
Kataoka T., Araki N., Nakano K., Matsuzaki Y. & Fukuyama H. Ductility of retrofitted RC columns with continuous fiber sheets. Non-metallic (FRP) Reinforcement for Concrete Structures, Proceedings of the Third International Symposium, Vol.1, Oct., 1997
The Building Center of Japan, Structural Regulations for Buildings - Building Standard Law Enforcement Ordinance, Chapter 3 explanation and operation, Dec. 1997
Uckan, E., Oven, V. A., & Erdik, M. (2002). A study of the response of the Mustafa Inan viaduct to the Kocaeli earthquake. *Bulletin of the Seismological Society of America February., 92*(1), 483–498.
Ye, L. P., Yue, Q. R., Zhao, S. H., & Li, Q. W. (2002). Shear strength of reinforced concrete columns strengthened with carbon-fibre-reinforced plastic sheet. *Journal of the Structural Engineering. American Society of Civil Engineers, 128*, 1527–1534.
Ye, L. P., Zhang, K., Zhao, S. H., & Feng, P. (2003). Experimental study on seismic strengthening of RC columns with wrapped CFRP sheets. *Construction and Building Materials, 17*, 499–506.
Zhou, Y., Chen, X., Wang, X., Sui, L., Huang, X., Guo, M., & Biao, Hu. (2020). Seismic performance of large rupture strain FRP retrofitted RC columns with corroded steel reinforcement. *Engineering Structures, 216*, 110744.

Publisher's Note

Moon-Sung Lee Associate Professor, Division of Architecture and Architectural Engineering, Hanyang University, ERICA Campus, Ansan, 15588, Korea

Li-Hyung Lee Professor, Department of Architectural Engineering, Hanyang University, Seoul, 04763, Korea